Microrheology of DNA hydrogels

Zhongyang Xing et al. 10.1073/pnas.XXXXXXXXXX

Supporting Information (SI)

A. Materials and Methods.

Oligonucleotide synthesis and Y-shaped DNA Hybridization. Oligonucleotides with 9 sticky bases were synthesized using the DNA synthesizer (BioAutomation MerMade-12, BioAutomation) followed by a HPLC purification process. They were stored in TE buffer (10 mM Tris, pH = 8.0, 1 mM EDTA, and 0 mM NaCl) at 4 °C. Equimolar quantities of the three corresponding strands were mixed in TE buffer solution with 200 mM NaCl to assist the DNA hybridization process. All mixtures were first denatured at 94 °C for 10 minutes, then slowly cooled down to 20 °C at a rate of -1 $°C\,s^{-1}$. Finally, we held it at 4 °C. The temperature control process was carried out using a PCR machine.

Oligonucleotides for bulk-rheology. For bulk-rheology and photographic realisations of the gels we used the same DNA sequences as those for the 9 sticky base pairs but with 7 and 12 bp overhangs, as well as the equivalents without the flexible T-spacers. All these oligonucleotides were purchased from were purchased from Integrated DNA Technologies.

UV-vis Spectroscopy Characterization. The melting temperature of Y-shaped building blocks was determined by measuring the 260 nm-peak absorbance of DNA mixture solution using UV-vis spectroscopy equipped with a temperature controlling system. Results showing the ionic effect can be found in section B.

DNA Hydrogels Preparation. DNA hydrogels were hybridized by mixing equimolar quantities of T-DNA and T'-DNA in TE buffer with a NaCl concentration of 200 mM. The melting temperature of the 9bp sticky ends, $T_{m2} = 37$ °C, was estimated using the nearest-neighbour model (1). The temperature was brought up to 45 °C for 20 minutes to break apart the sticky ends and retain the Y-shaped structure at the same time. Subsequently, the sample was cooled down slowly at a cooling speed of 0.02 °C/s to 10 °C. Then, the sample was kept at 4 °C until reused in the next measurement.

Tracer Particles. We used 600 nm and 230 nm polystyrene particles as tracer particles. The 230 nm particles were synthesised and densely coated with PEG chains for stabilisation following a protocol described by M. Zupkauskas *et al* (2). The 600 nm particles were charge stabilised via carboxylic surface groups and provided by LS Instruments AG.

Sample loading. We added 1% tracer particles into the T-DNA and T'-DNA solutions respectively, and then mixed them up thoroughly. The final samples were loaded into transparent cuvette holders (optical path length = 1 mm) for use in DWS measurements.

Diffusing Wave Spectroscopy Measurements. Diffusing-wave spectroscopy measurements were performed on a commercial DWS instrument (DWS RheoLab, LS Instruments AG) in transmission mode. A 10 mm wide an 1 mm thick cuvette was used as sample cell and the temperature was controlled within ± 0.2 °C. Calibration measurements were performed on deionized water with the 1 % w/v of the same tracer particles and the same cuvette to acquire the transport mean free path l^* for the setting used. Scattering measurements were performed by the machine, outputting an intensity correlation function to a PC for further analysis of the data.

Bulk-rheology. Bulk-rheology measurements were performed using an Anton Paar MCR500 rheometer with true-gap technology in the cone-plate geometry. In all measurements we used a cone with 25 mm diameter and inclination of 1°. We used a custom-made cover to minimize evaporation during the measurements.

B. Estimate of the melting temperature of Y-shaped body.

The melting temperature of dsDNA is estimated by computing the hybridization free energy, ΔG^0, of the complementary sequences, which can be predicted using the unified nearest-neighbor (NN) thermodynamics model (1). In the NN model, ΔG^0 is computed by summing up the standard free-energy contributions of all neighbouring bases in a DNA sequence, respecting the orientation of the two complementary ssDNA running antiparrallel, plus an initiation energy and the energy contributions coming from the 'dangling ends'; the salt concentration is also taken into account. The enthalpy, ΔH^0, and entropy, ΔS^0, of the strands can be calculated via tabulated values accordingly, and they relate to the Gibbs free energy using Eq 1:

$$\Delta G^0 = \Delta H^0 - T\Delta S^0. \quad [1]$$

The melting temperature, T_m, at which half of the double-helical strands are melted, can then be predicted using Eq 2 (1):

$$T_m = \frac{\Delta H^0}{\Delta S^0 + R\ln(\rho/2)}, \quad [2]$$

where R = 1.978 cal/Kmol is the gas constant, and $\rho = \rho_{AA'} = \rho_A = \rho_{A'}$ is the concentration of the dsDNA, when all ssDNAs are hybridized. An empirical salt concentration effect is also included as a compensation in ΔG^0.

However, the T_m of our structure is influenced by further factors: (i) Since three arms are joined together in our Y-shapes, they should not be treated as independent double helices; (ii) di Michele et al. (3) have shown that inert tails on dsDNA (here the sticky overhangs) cause a decrease in melting temperature by about 3 °C to 7 °C, depending on the length of these inert tail; (iii) The solvent conditions will also influence T_m. In this study we used TE buffer (10 mM Tris, 1 mM EDTA, adjusted to pH 8.0 with HCl) to stabilise the DNA. For instance, the T_m of a given complementary pair AA' in TE buffer is different to that in de-ionized water (see section C). The analytical approach to comprise all these effects in Eq 2 is unavailable, but we can combine the experimental measurements and the NN model routine to estimate the melting curves for experimental conditions that do not allow a direct measurement of T_m.

Table S1 lists the calculated melting temperatures of three arms for an added NaCl concentration of 150 mM and a total ssDNA concentration of 1 µM based on the NN model. We took the average melting temperatures of these arms as the melting temperature of the Y-shaped body as the starting point, i.e. $T_m^{Y-shape} = \frac{1}{3}(T_m^{arm1} + T_m^{arm2} + T_m^{arm3}) \approx 55.02$ °C. This is comparable to the experimentally measured melting temperatures for T-DNA and T'-DNA described in the main text, which indicates that the three factors mentioned above can compensate each other in our case. Similarly, we estimated the averaged melting temperature of the Y-shaped body at the working condition ([NaCl]=200 mM, [ssDNA]=500 µM, in TE buffer) being 68.64 °C.

C. Experimental measurements to test ionic effects on melting temperatures. To demonstrate the ionic effects on the melting temperatures of the Y-shaped DNA formation, we performed absorbance spectroscopy measurements at 260 nm on samples with varying concentrations of added NaCl and the buffer test (figure S1). The 260 nm wavelength absorbance measurements were performed on a Varian Cary 300 bio UV-Visible spectrometer equipped with a Peltier stage for temperature controlling. 700 µl of sample solutions were injected into quartz cuvettes and sealed with teflon lids (Hellma Analytics) to avoid evaporation at high temperatures.

NaCl concentration effect. For the NaCl concentration test, we used the oligonucleotides with complementary strands (black-colored) and inert tails (red-colored) that do not hybridize at RT:

1. 5'- TGT CAC TCA CAG TGG ATC CGC ATG ATC CAT TCG CCG TAA GTA - 3'
2. 5'- TGT CAC TCA CAG TAC TTA CGG CGA ATG ACA CCG AAT CAG CCT - 3'
3. 5'- TGT CAC TCA CAGAGG CTG ATT CGG TGT GAT CAT GCG GAT CCA - 3'

An equimolar amount of each strand was dissolved in TE buffer with the final DNA concentration at 1 µM for each type, and NaCl concentrations varying between 0 mM, 50 mM, 100 mM and 150 mM.

Buffer effect. Samples were measured in deionized water (blue lines) and TE buffer (red lines) respectively for comparison. 150 mM NaCl was added to both solutions to screen the negative charges on the DNA phosphate backbones.

Samples were first heated up to 85 °C and incubated for 20 minutes, followed by a cooling ramp down to 20 °C at the rate of 0.2 °C/min. After another 20 minutes incubation at 20 °C, a heating ramp was ran for the hysteresis test. From the results presented in figure S1, the melting temperature increases with increasing added salt concentration. A weak hysteresis is seen, which is insignificant in comparison to other effects, such as base-pair mismatches due to impurities of the hybridized DNA. Hence, it is essential to use PAGE purified DNA to obtain accurate temperature dependent viscoelastic properties.

D. Polyacrylamide Gel Electrophoresis. To check the efficiency of the Y-shaped DNA hybridization, we performed polyacrylamide gel electrophoresis (PAGE)(4) with a 10 % gel. The gel was prepared using acrylamide/bis-acrylamide solution (30 %, Sigma-Aldrich ®) and TBE buffer (Tris-Borate-EDTA buffer, 10× concentration, Sigma-Aldrich ®), with TMEDA (N,N,N',N'-Tetramethylethylenediamine, Sigma-Aldrich ®) and APS (Ammonium persulfate, 10 %, Sigma-Aldrich ®) added to catalyze the polymerization of acrylamide. 0.5 × TBE buffer was used as running buffer. $MgCl_2$ was added to both the gel and the running buffer at the final concentration of 11 mM, in order to stabilize the hybridized DNA structures during the electrophoresis process.

The loading sample contains 50 ∼ 250 ng DNA strands in total and 1× gel loading dye (Purple, New England BioLabs ®) per lane. DNA ladders were loaded into lane 5 (Low Molecular Weight DNA Ladder, New England BioLab ®) and lane 10 (50 bp DNA Ladder, purchased from New England BioLab ®) to scale the migration of the DNA samples in the parallel lanes (figure S2). The specific sequences used for PAGE are listed in table S2: f_1, f_2 and f_3 are the components of T-DNA; f_{p1}, f_{p2} and f_{p3} are for T'-DNA. So $f_{(p)i}$ and $f_{(p)j}$ $(i, j = 1, 2, 3$ and $i \neq j)$ are partially complementary to each other, and therefore can hybridize together at room temperature. Lanes 1-3 were loaded with the mixture of f_i and f_j $(i, j = 1, 2, 3$ and $i \neq j)$ at 1:1 molar ratio , and lane 4 was loaded with the mixture of f_1, f_2 and f_3 at 1:1:1 molar ratio. Lanes 6-8 were loaded with the mixture of f_{p1} and f_{pj} $(i, j = 1, 2, 3$ and $i \neq j)$ at 1:1 molar ratio, and lane 9 was loaded with the mixture of f_{p1}, f_{p2} and f_{p3} at 1:1:1 molar ratio. The samples were electrophoresed at 100 V for 90 min at room temperature.

The electrophoresis results are shown in figure S2. The sharp and distinct principle bands in lanes 1-4 and lanes 6-9 show a high-yield hybridization of DNA complexes. The principle bands in lane 1-3 and 6-8 were near the position of the 50 bps marker in lane 10, in accordance with the mass of the two hybridized ssDNAs (46 bases per ssDNA). The dark bands in lane 4 and lane 9 represent the migration of the T-DNA and T'-DNA complexes respectively.

E. DWS measurements with 230 nm PS beads on cooling and heating ramps. We also conducted the DWS measurements using 230 nm PS particles as probe beads, following the same routine as for the the measurements with 600 nm beads. The sample was 1.4 - 2 v/v % Y-shaped DNA (a **T**-DNA/**T'**-DNA concentration of 500 µM),containing 1 v/v % concentration of the colloids. Cooling down and measurements were taken starting from 50 °C to 17 °C at an interval of 1 °C. As expected, the decay time increases as the temperature goes down.

The ICF data for the cooling and heating ramps are shown in figure S3 **A**. They are in good agreement with each other, indicating the thermal reversibility of the DNA hydrogen bonds between sticky ends.

MSD results converted from the intensity correlation functions are shown in figure S3 **B**. *Top* and *bottom* figures present the temperature-evolution of the MSDs for cooling and heating ramps respectively. Both show a similar trend, confirming that the system shows little hysteresis. The MSD curves show a temperature dependence that is very similar to that of the samples measured with the same overall Y-DNA concentration but with 600 nm tracer particles. These results demonstrate that we measure with DWS the physical behaviour of our DNA hydrogels, and are not influenced by the nature of the tracer particles used.

The elastic G'(ω) and viscous moduli G"(ω) extracted from the MSD data are shown in figure S4 . As expected, the results for 230 nm tracer particles correspond to the ones obtained with 600 nm trace particles shown in the main text.

F. Time evolution DWS measurements. To ensure the DNA hydrogel sample stays at its equilibrium state during the DWS measurements duration, we performed a series of time evolution experiments for the sample at the time sequences up to 25 minutes after loading, at temperatures ranging from below to above the melting-transition region. All measurements were performed on the DNA hydrogel sample at the **T**-DNA/**T'**-DNA concentration of 500 µM with 1 v/v % 230 nm sterically stablised polystyrene particles. Intensity correlation functions (ICF) on various temperatures were obtained after 1, 3 , 5 , 7 , 10 , 15 and 25 minutes waiting time respectively after bringing the sample to a given temperature (S5). Figure S6 shows the half-decay times extracted from the ICF results, showing the changes with temperature. Each data point was averaged over seven measurements at different times, and the error bar represents the statistic error. The results show that the ageing effect is minor compared to the temperature effect.

G. Microrheology: data analysis. Data analysis is performed via custom routines written in MATLAB (R2016b). The raw autocorrelation curves obtained by DWS measurements are fitted to a multiexponential function of the form:

$$g_1(\tau) = \sum_i a_i e^{-\Gamma_i \tau} \quad [3]$$

The form of the fit is motivated by the fact that the autocorrelation function $g_1(\tau)$ for the detector geometry adopted is nearly exponential and is thus expected to be well represented by the chosen functional form (5). The parameters a_i and Γ_i are obtained via the well known CONTIN method (6). The mean-square displacement (MSD) $\langle \Delta r^2(\tau) \rangle$ is obtained from the fitted autocorrelation curves by inverting the following equation (5) and solving for x:

$$g_1(\tau) = \frac{\frac{L/l^*+4/3}{a^*+2/3} \sinh(a^* x) + 2/3\, x \cosh(a^* x)}{(1+4/9\, x^2)\sinh(L/l^*\, x) + 4/3\, x \cosh(L/l^*\, x)} \quad [4]$$

where $x = \sqrt{q_0^2 \langle \Delta r^2(\tau) \rangle}$, $a^* = z_0/l^*$, z_0 is the distance into the sample from the incident surface to the place where the diffuse source is located (calibration parameters outputted from the DWS setup), $q_0 = 2\pi n_s/\lambda$ is the photon wave vector in the solvent, λ is the laser wavelength, n_s is the index of refraction of the solvent and L is the cuvette thickness.
The MSD curves are converted into the complex modulus $G^*(\omega)$ by direct conversion following the approach by Evans and expanded by Tassieri (7).

H. Macroscopic modelling of the Y-DNA hydrogel structures. To allow for a better understanding of the possible formations of the network and its elasticity, we fabricated macroscopic DNA hydrogel models using laser cut Y-shaped unit representing the more rigide Y-shaped DNA building blocks and heat-shrinkable yellow tubes as the more flexible connectors. The laser-cut unit has three arms are in a plane (as predicted by various models), and are at an angle of 120 ° to each other. They were made of hard plastic to reflect the fact that short dsDNA behave like rigid rods (the persistence length of dsDNA is about 50 nm, corresponding to 150 base pairs). We used transparent and blue Y-shapes to represent the T-DNA and T'-DNA respectively. Due to some flexibility of the yellow rubber connectors, the structure is allowed to twist or blend slightly thus simulating the bigger flexibility of the link between Y-shapes, which is provided by the flexible linkers (2 time 4 unbound thymines). Note that the persistence length of ssDNA is only 1nm corresponding to 3 base pairs. Further, obeying the fact that dsDNA will hybridize into a polymer chain with a twist and pitch given by every added base-pair one can impose a prescribed rotational angle between a Y' and a Y'-shape, assuming that we have initially no flexible linker. Choosing for our 9 bp sticky ends to bind the two flat Y-shapes under rotational angle of 90° we obtain the open, 3d-networks shown in Figure S7 **A, i-ii**. Adding one more base pair to the total distance between the centers of two Y-shapes will change their relative twist. Playing with the correct connectors more ordered cages can be designed (Figure S7 **A, iii-v**). Using a system with no flexible linkers but different linker length will lead to very inhomogeneous networks with many arms that will not necessarily be able to hybridize due to topological constraints. And also the overall elasticity will be influenced.

I. Bulk-rheology. To demonstrate the effect of the flexible linkers, we performed bulk-rheology measurements on the **T** and **T'**-DNA system with the 9bp long sticky overhangs, both with and without flexible linker. We compared these with the very same system (same concentration) but with 12 bp overhangs - again with and without flexible linkers (Figure S7 **B**). In order to avoid too much evaporation during the measurements we preheated the lower plate of the rheometer to 30 °C with the cone in close proximity, then lifted the cone to quickly place the gel and immediately afterwards lowered the cone to measuring position. The geometry was then enclosed with a vapour trap. After a 10-minute equilibration time we lowered the system's temperature to 20 °C. This procedure does not allow for careful equilibrium hybridization of the sticky overhangs and as we loaded the samples in the gel state they had been strongly sheared, but slow cooling form 50 to 20 °C would compromise our samples. Nevertheless, the bulk-rheology results closely match the results obtained with DWS at low frequencies for the 9bp overhang system with flexible linker, showing a bulk-elasticity plateau at around 200 Pa. And also G"(ω) dips down slightly at higher frequencies, as was observed in the DWS measurements. When further cooling the sample to 10 °C both moduli do not change much. In fact the plateau value of G'(ω) only increases by a few percent, which illustrates that although we loaded the sample in a crude way, we control the systems elasticity purely by the *known* number of crosslinks we add to the system, which are all connected to each other at 20 °C. The exciting only change we achieve is by removing the flexible linkers leading to the increase of the elasticity plateau to about 500 Pa. As explained in the main text, this is due to the fact that by the removal of the flexibility in the system we transfer the system from a transient network of flexible linkers dominated by entropy to a more rigid energy driven network.

Comparison with the same system, in which we replaced the sticky overhangs with 12 bases (5'- TGT CAC TCA CAG and 5'- CTG TGA GTG ACA for the **T** and **T'**-DNA shapes) respectively showed a very similar behaviour. As for the system with 9 bases overhangs we measure a similar bulk elasticity

of about 90 Pa when incorporating the flexible linkers, which increased now by a factor of 7 when the flexible linker is removed. Note that although the systems transition to a gel occurs now at even higher temperatures (for details see below) while keeping the concentration of the linkers the same we still obtain a very similar bulk elasticity. The small variations i value at 20 °C is simply due to the loading procedure and the fact that in bulk-rheology each loading can lead to variations of about 10% because every time a slightly different amount may be used. The striking result is the increase in G'(ω), which is purely due to the absence of the flexible linkers.

J. DWS microrheology on mixtures with 12 bases overhangs and flexible linkers. To test our hypothesis that the melting temperature of the sticky overhangs between the Y-shapes coincides with the percolation transition we also performed DWS measurements on a mixture of Y-DNA and Y'-DNA but with 12 bases sticky overhangs, still including the flexible thymine linkers. UV-vis adsorption measurements of these 12 bases linkers gave a melting temperature of $T_m = 48$ °C for the pure overhangs (not shown here), which is still lower than the melting transition of the Y-shapes. Following the same melting and heating protocol as for all other micro-rheology measurements but heating now to 58 °C, and using 600 nm large PS probe particles we obtained a similar behaviour as for the system with 9 bases sticky overhangs. Characteristic G'(ω) and G"(ω) curves, extracted from the DWS data, for three different temperatures are given in Figure S8. The system was at 31°C already in the gel phase, while the viscose modulus dominated in the liquid state of the Y-shapes at 58 °C. And similar to the 9 bases overhang system, the overall viscosity was a factor 100 higher than that of pure water. At around 44 °C we again observed the same behaviour of G'(ω) and G"(ω) running parallel and on top of each other, which we identified as the onset of percolation. This is close to the melting temperature measured for the pure 12 bases overhangs, which we expect to drop by a couple of degrees when the long Y-shapes are attached.

1. SantaLucia J (1998) A unified view of polymer, dumbbell, and oligonucleotide dna nearest-neighbor thermodynamics. *Proceedings of the National Academy of Sciences* 95(4):1460–1465.
2. Zupkauskas M, Lan Y, Joshi D, Ruff Z, Eiser E (2017) Optically transparent dense colloidal gels. *Chemical Science*.
3. Di Michele L, et al. (2014) Effect of inert tails on the thermodynamics of dna hybridization. *Journal of the American Chemical Society* 136(18):6538–6541.
4. Barril P, Nates S (2012) Introduction to agarose and polyacrylamide gel electrophoresis matrices with respect to their detection sensitivities in *Gel Electrophoresis-Principles and Basics*. (InTech).
5. Pine D, Weitz D, Chaikin P, Herbolzheimer E (1988) Diffusing wave spectroscopy. *Physical review letters* 60(12):1134.
6. Štěpánek P, Brown W, Hvidt S (1996) Relaxation of concentration fluctuations in a shear field. *Macromolecules* 29(27):8888–8893.
7. Tassieri M, Evans R, Warren RL, Bailey NJ, Cooper JM (2012) Microrheology with optical tweezers: data analysis. *New Journal of Physics* 14(11):115032.

Table S1. The sequences of dsDNA arms

name	sequences	predicted T_m (@[NaCl]=150 mM, [DNA]=1 μM)	predicted T_m (@[NaCl]=200 mM, [DNA]=500 μM)
arm 1	5'- TGG ATC CGC ATG ATC - 3' 3'- ACC TAG GCG TAC TAG -5'	55.27 °C	68.91 °C
arm 2	5' - TAC TTA CGG CGA ATG - 3' 3' - ATG AAT GCC GCT TAC - 5'	52.47 °C	65.69 °C
arm 3	5'- AGG CTG ATT CGG TGT - 3' 3' - TCC GAC TAA GCC ACA - 5'	57.34 °C	71.31 °C

Table S2. The oligonucleotides sequences of PAGE loading samples

name	sticky end	free joint	segment I	segment II
f_1	5'- TGT CAC TCA CAG	TTTT	TGG ATC CGC ATG ATC	CAT TCG CCG TAA GTA -3'
f_2	5'- TGT CAC TCA CAG	TTTT	TAC TTA CGG CGA ATG	ACA CCG AAT CAG CCT -3'
f_3	5'- TGT CAC TCA CAG	TTTT	AGG CTG ATT CGG TGT	GAT CAT GCG GAT CCA -3'
f_{p1}	5'- CTG TGA GTG ACA	TTTT	TGG ATC CGC ATG ATC	CAT TCG CCG TAA GTA -3'
f_{p2}	5'- CTG TGA GTG ACA	TTTT	TAC TTA CGG CGA ATG	ACA CCG AAT CAG CCT -3'
f_{p3}	5'- CTG TGA GTG ACA	TTTT	AGG CTG ATT CGG TGT	GAT CAT GCG GAT CCA -3'

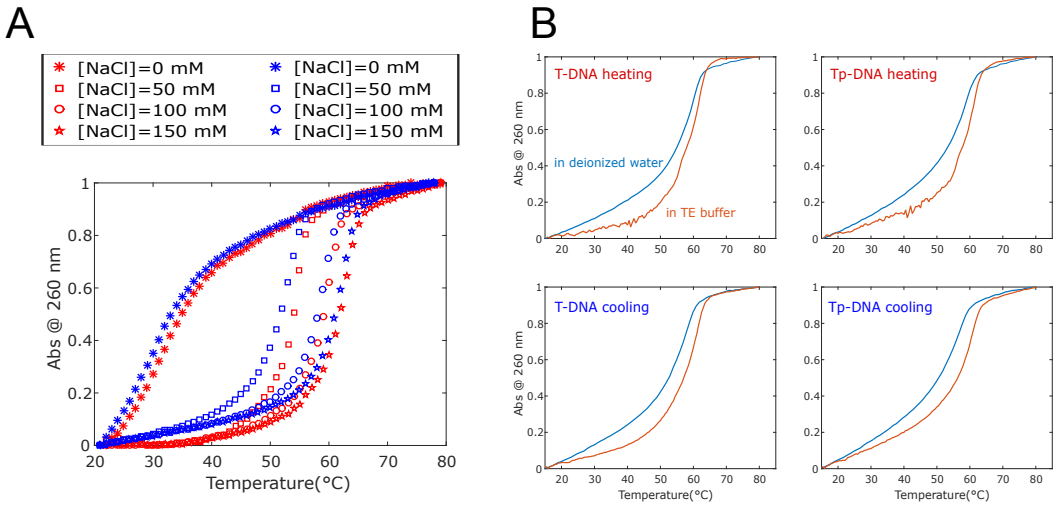

Fig. S1. (A) Rescaled absorbance profiles for a sample with Y-shaped architecture, no free joint; in all cases we used a TE buffer (10 mM Tris, bring to pH 8.0 with HCl, 1 mM EDTA), and added NaCl at various concentrations. Red and blue symbols are experimental data obtained for a heating and cooling process, respectively. Melting temperatures can be extracted from the crossovers between the absorbance curves and the horizontal dashed line. (B) Rescaled absorbance profiles for T-DNA and T'-DNA hybridization in deionized water (blue lines) and TE buffer (red lines).

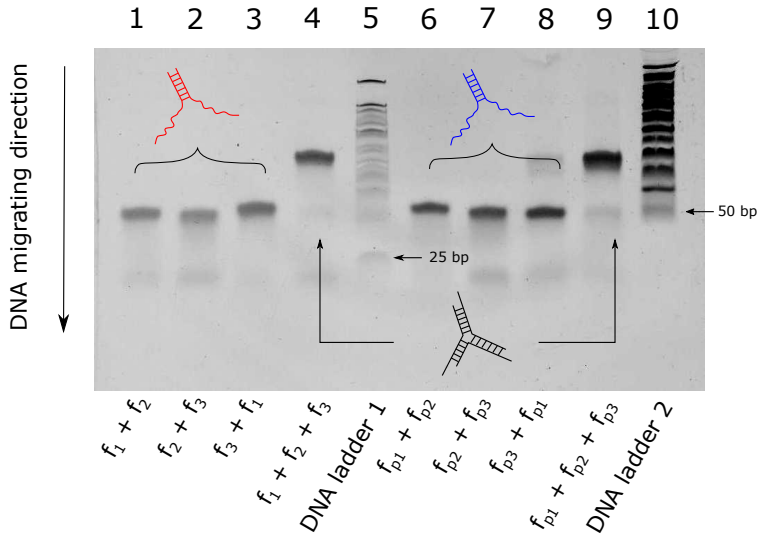

Fig. S2. Polyacrylamide gel electrophoresis characterization of various ssDNA mixutres.

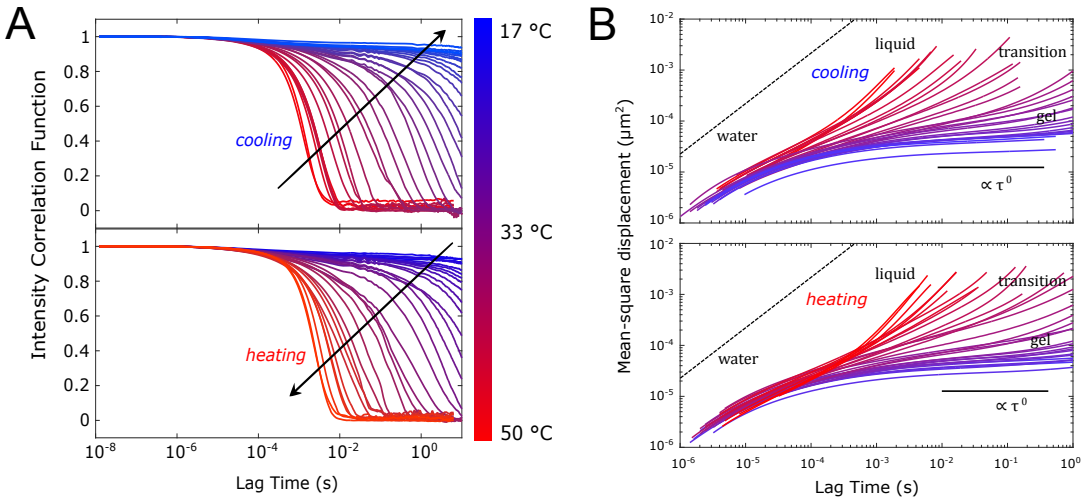

Fig. S3. (A) The temperature-dependent intensity-correlation function (ICF) data measured from the described DNA hydrogel sample containing 1 v/v % of 230 nm sterically stablised polysterene particles. *Top* The cooling ramp for the temperature ranging from 50 °C to 17 °C (from the red lines to the blue lines), and *bottom* the corresponding heating ramp . (B) Mean-square displacements (MSD) extracted from the ICF curves. The dashed lines are the theoretical MSD curves for the tracer particles at room temperature in pure buffer solution, shown as reference. The gray regions in the plots indicate the melting-temperature transition region.

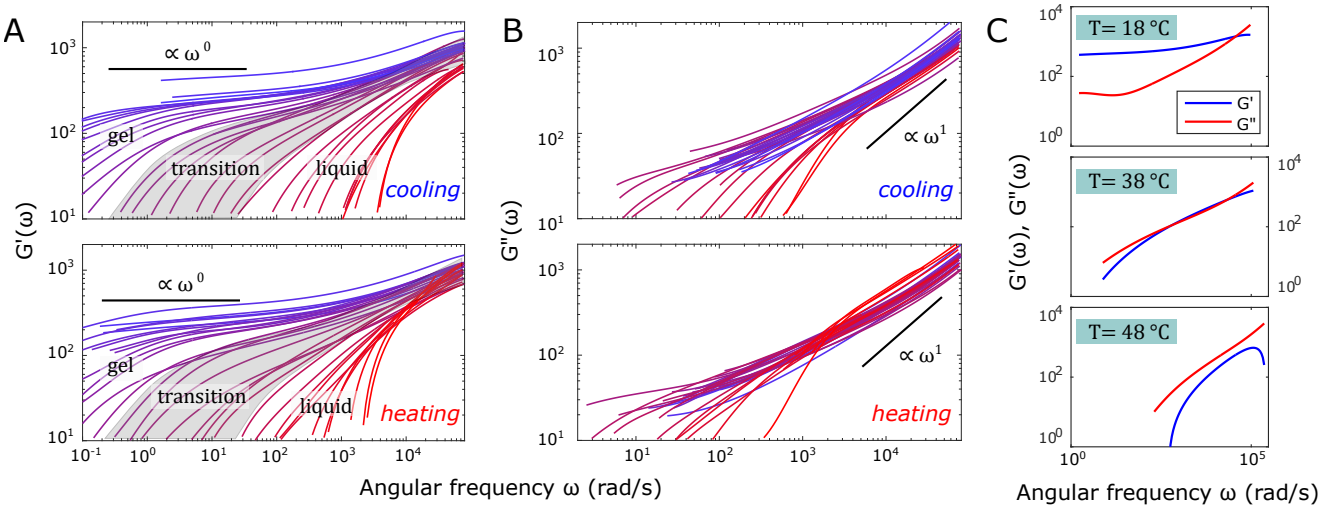

Fig. S4. Temperature-evolution of the complex moduli $G'(\omega)$ and $G''(\omega)$ as a function of frequency extracted from the MSDs in Fig. S3. (A) The elastic moduli $G'(\omega)$ measured in cooling and heating ramps. At temperatures above T_{m2}, G' drops down at a frequency below $10^2 \sim 10^4 rad/s$, showing close-to-zero elasticity; below T_{m2}, only th e onset of the decay in the ICF could be monitored. (B) The viscous modulus $G''(\omega)$ in cooling (*top*) ramp. (C) Comparison of $G'(\omega)$ and $G''(\omega)$ at temperatures of 18 °C, 38 °C, and 48 °C, representing typical behavior at temperatures below, around, and above T_m. At 18 °C, G'' is higher than G' at frequencies below the crossover frequency $\sim 10^4$ rad/s; at 38 °C, G' and G'' are overlapping over almost the entire frequency range; at 48 °C, G'' is higher than G' over the whole measurable frequency range, showing no crossover point at all.

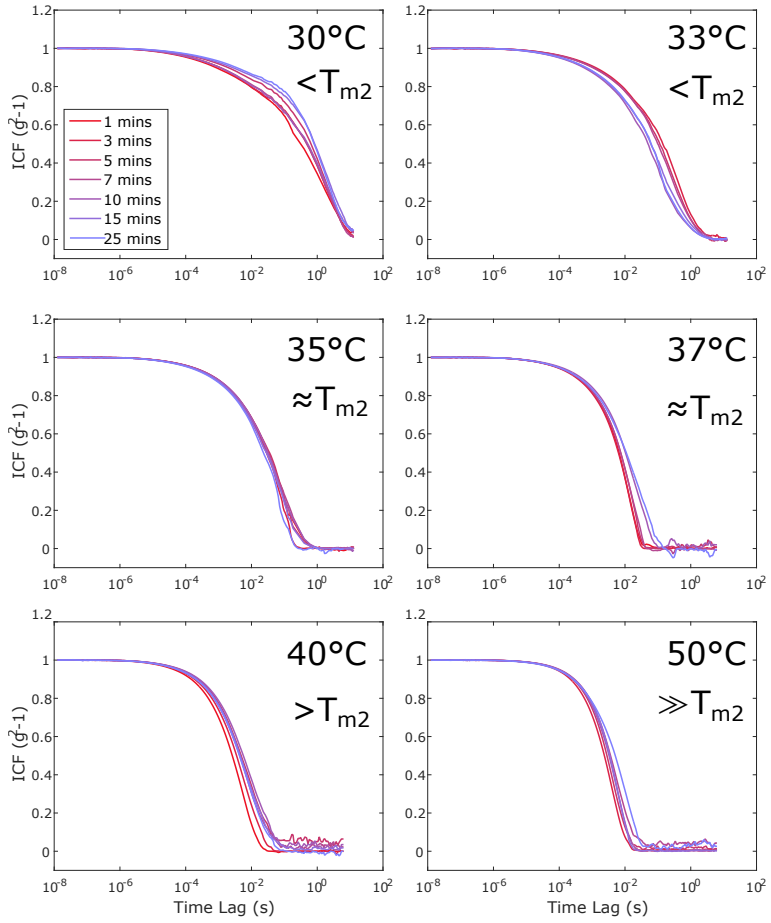

Fig. S5. Aging effects at different temperatures. All figures are obtained from the DNA hydrogel sample with a DNA concentration of 500 μM using 230 nm sterically stablised polystyrene particles. The intensity correlation functions (ICF) were measured 1, 3, 5, 7, 10, 15 and 25 minutes directly after placing the sample into the cell.

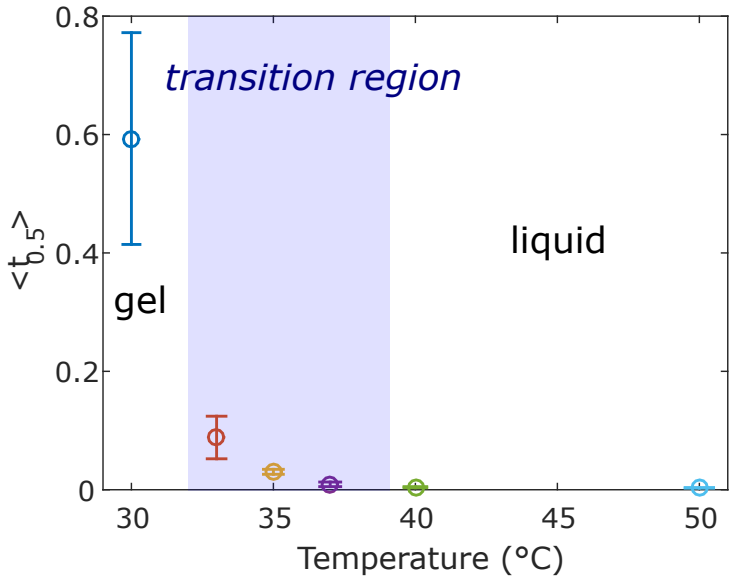

Fig. S6. Half-decayed time point extracted from ICF results against temperature. The transition region is marked in blue region. The region on the left is the gel state and on the right is the liquid state.

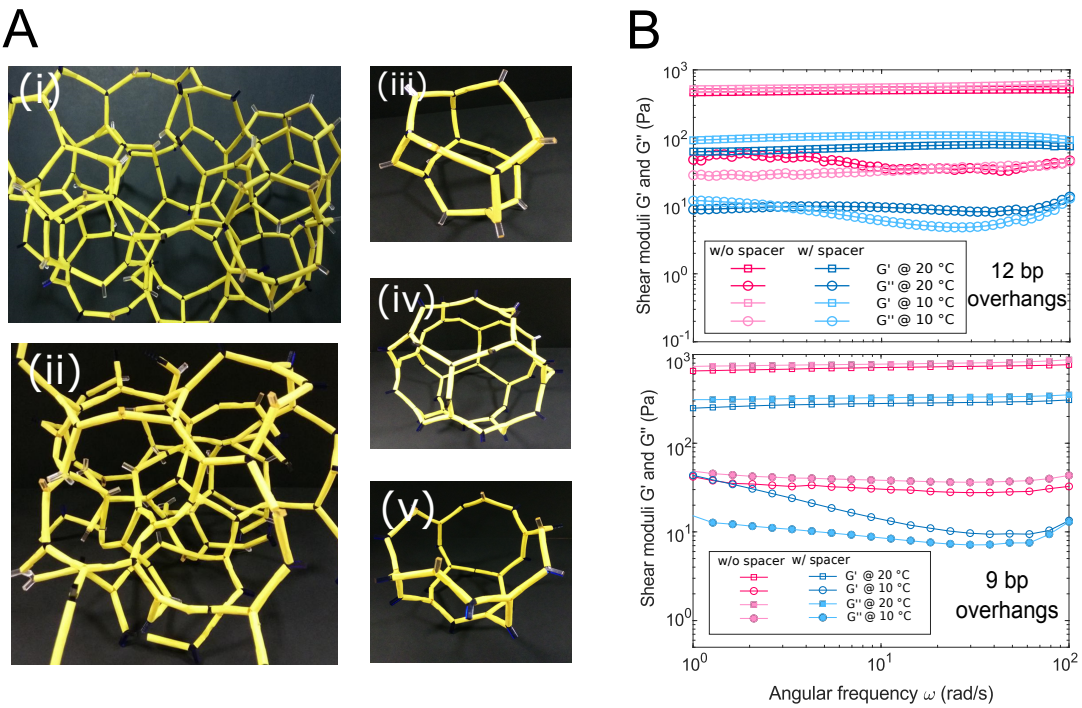

Fig. S7. (A) Macroscopic representatives of microscopic the DNA hydrogel structures. **i** Semi-flexible gel structure. **ii** Disordered structure with many bonds disconnected. **iii - v** Highly symmetry subunit model representing a cube, a dodecahedron, and an open cap respectively. (B) Bulk-rheology measurements on 500 μM concentrations of **T** and **T'**-DNA nanostars *top* for sticky overhangs with 12-bases and *bottom* the same 9bp overhangs used in all microrheology measurements presented. Also the same buffer and salt conditions were used.

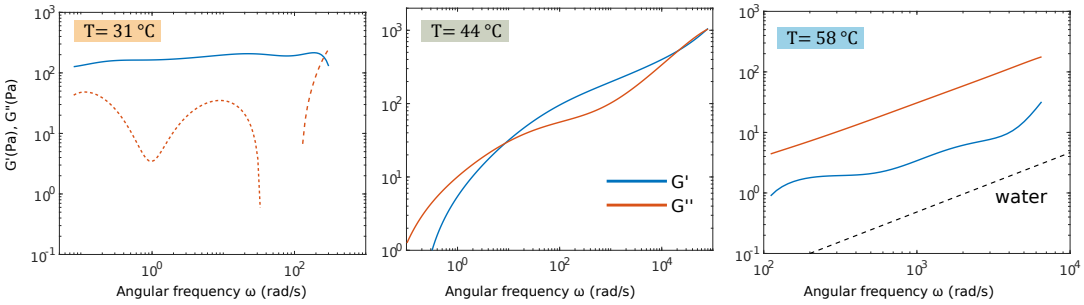

Fig. S8. G'(ω) and G"(ω) curves extracted from DWS measurements on 500 μM concentrations of **T** and **T'**-DNA nanostars for sticky overhangs with 12 bases overhangs and flexible linkers. The same buffer and salt conditions were used as or the system with 9 bases overhangs and flexible spacers. For clarity we only show 3 temperature sets, depicting the shear moduli in the gel (31°C), the percolation (44 $^{\circ}$C) and the liquid state (58 $^{\circ}$C).